ACS APPLIED ENERGY MATERIALS

www.acsaem.org

Article

Photoelectrochemical Generation of Value-Added Organics via C−H Bond Activation at WO_3 Photoelectrodes

Andrea Mantovani, Edoardo Marchini, Anna Ianniello, Agnese Amati, Stefano Caramori, and Mirco Natali*

Cite This: *ACS Appl. Energy Mater.* 2025, 8, 18355−18362

Read Online

ACCESS | Metrics & More | Article Recommendations | Supporting Information

ABSTRACT: The production of value-added molecular scaffolds using sustainable routes and mild conditions currently represents an important challenge in chemical sciences. In the present work, we report on the oxidation of cyclohexane (CH) to cyclohexanol (CH-ol) and cyclohexanone (CH-one) and of tetrahydrofuran (THF) to 2-hydroxotetrahydrofuran (2HTHF) and gamma-butyrolactone (GBL) by exploiting WO_3 electrodes and visible light. Photoelectrochemical experiments as well as transient absorption spectroscopy measurements were performed to investigate the relevant mechanistic aspects associated with these reactions. For this purpose, we also compare the activity of two different electrode types: one obtained by deposition of a colloidal suspension (type I) and one prepared via solvothermal synthesis (type II). We show that, while production of CH-ol and CH-one is comparable with both electrodes (total Faradaic efficiencies in the order of 30% after 6 h of irradiation at an applied bias of +1.15 V vs Fc^+/Fc), more efficient formation of 2HTHF and GBL can be achieved using type I electrodes (total Faradaic efficiencies up to 90% for type I electrodes after 6 h of irradiation at an applied bias of +1.45 V vs Fc^+/Fc in comparison to values of ca. 30% for type II electrodes). The different behaviors can be rationalized on the basis of the different morphologies and structural characteristics of the two WO_3 materials, highlighting the strong relationship between material design and target reaction. All in all, this study presents a synthetic strategy that expands the application of WO_3 beyond its conventional aqueous-phase use, enabling the profitable oxidation of organic substrates into value-added products.

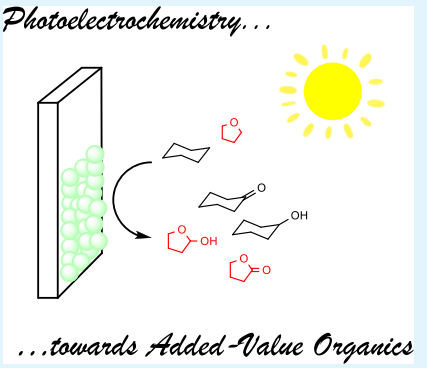

KEYWORDS: *tungsten oxide, cyclohexane, tetrahydrofuran, photoelectrochemistry, photoxidation*

INTRODUCTION

In the field of sustainable chemistry, there is an increasing demand toward the development of novel, safe, and environmentally friendly processes that enable the synthesis of molecules of industrial and pharmaceutical interest featuring specific reactivity and functionalities.[1−6] Within this framework, the selective generation of value-added organics using abundant and non-toxic materials and light currently represents a viable solution.[7−10] In this regard, the photoelectrochemical oxidation of cyclohexane (CH) to cyclohexanol (CH-ol) and cyclohexanone (CH-one), known as KA oil mixture, as well as the selective conversion of tetrahydrofuran (THF) into gamma-butyrolactone (GBL) represent promising routes toward molecular precursors for the synthesis of chemicals of significant industrial interest.[11−20] These reactions can occur via C−H bond activation with the formation of a carbon radical, followed by reaction with dioxygen delivering a peroxyl radical. Reaction between two peroxyl radicals then leads to the alcohol and ketone products.[21−24] While simple at first glance, this reaction poses significant hurdles associated with the large energetic requirements for the homolytic cleavage of the C−H bond (bond dissociation energies, BDEs, of 99 and 92 kcal·mol^{-1} for CH and THF, respectively). For these reasons, harsh experimental conditions such as high temperature and pressures are typically required to accomplish these reactions,[25,26] resulting in large costs and weakly sustainable processes.

The merging of heterogeneous catalysis and light can be instead employed to achieve substantial reactivity with a parallel positive impact on the environment. Following this concept, TiO_2 nanoparticles were employed to perform the light-driven oxidation of CH in different solvents,[27] while Se-doped TiO_2 was considered for the oxidation of THF to GBL.[28] Though operative, the extended applicability of these systems is impeded by the light-harvesting ability of TiO_2, which is limited to the UV portion of the solar spectrum. For this reason, a recent strategy for the oxidation of CH was considered based on the use of composite $Ni_3V_2O_8$-gCN

Received: October 21, 2025
Revised: November 18, 2025
Accepted: November 20, 2025
Published: November 28, 2025

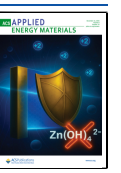

nanoparticles. Upon light irradiation, selective formation of CH-one was observed.[29] In a similar approach, WO_3 nanoparticles loaded with Pt were employed to selectively oxidize CH to CH-ol and CH-one.[30] The origin of the high selectivity was attributed to the ability of Pt to suppress the formation of superoxide, thereby limiting further oxidation of these products. A photoelectrochemical strategy was also recently envisioned for the oxidation of CH using visible light and WO_3 photoanodes.[31] This study was, however, conducted in a complex electrolyte solution composed of *t*BuOH and concentrated HNO_3, thus, limiting potential large-scale applications.

Based on these findings, the present work targets the investigation of both the oxidation of CH to CH-ol and CH-one and of THF to 2-hydroxotetrahydrofuran (2HTHF) and GBL under mild conditions combining visible light and WO_3 photoelectrodes (Scheme 1a). In particular, two different types of electrodes were considered, differing for both the preparation method and the resulting morphology (Scheme 1b), showing that the reaction outcome and yield strictly depend on the nature and characteristics of the material. A detailed photoelectrochemical and spectroscopic characterization of the WO_3 photoanodes under operative conditions was finally performed to rationalize the observed behavior and extract mechanistic information. Notably, this work introduces a novel approach by extending the application of WO_3 beyond their conventional domain toward the selective oxidation of organic compounds into value-added products.

Scheme 1. (a) Schematic Representation of the Photoelectrochemical Oxidation Processes Studied in This Work; and (b) Principal Characteristics of Type I and II Electrodes Employed for the Oxidation of CH and THF

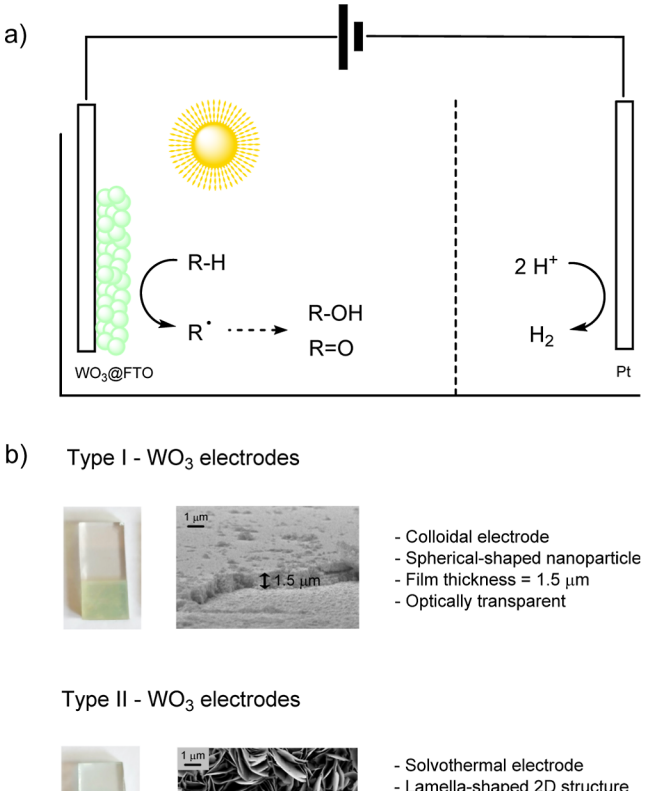

EXPERIMENTAL SECTION

Materials and Methods. All reagents were obtained from standard suppliers and used without additional purification. The preparation and detailed structural and morphological characterization of the employed WO_3 electrodes are reported elsewhere (see refs 33 and 34 for the colloidal type I electrodes and refs 35 and 36 for the solvothermal, type II electrodes). An electrochemical grade acetonitrile solvent was employed. THF was employed after distillation over Na and benzophenone, following an established procedure.[32] Photocurrent density−voltage curves ($J-V$) and bulk electrolysis measurements were carried out using an Autolab PGSTAT 302 N potentiostat in a three-electrode configuration using an Ag wire as a quasi-reference and a Pt counter electrode. Potentials were then converted versus Fc^+/Fc by recording a CV in the presence of ferrocene added as an internal standard. A three-chamber cell was used with all of the compartments separated by a frit (see Figure S1). The cell was irradiated with an Abet solar simulator equipped with an AM1.5G filter adjusted to 1 sun (0.1 $W{\cdot}cm^{-2}$) by means of a Newport 1918 C Power Meter. IPCE was measured in a three-electrode configuration under monochromatic illumination generated by an air-cooled Luxtel 175 W Xe lamp coupled to an Applied Photophysics monochromator. An applied potential of +1.15 and +1.45 V vs Fc^+/Fc was applied for the measurements in acetonitrile and THF, respectively. Incident irradiance was measured with a calibrated silicon photodiode. EIS measurements were carried out over a wide potential range. The signal amplitude was equal to 10 mV with a frequency range from 10^5 to 10^{-1} Hz, while the impedance of the photoanode was sampled each 50 mV. Quantification of CH-ol, CH-one, 2HTHF, and GBL was performed by analyzing the anodic compartment at 3 and 6 h using an Agilent 6890 gas chromatograph equipped with a FID detector and a (5%-phenyl)-methylpolysiloxane column. Calibration was performed using the external standard method by injecting known volumes of pure analyte. Absorption spectra were recorded at room temperature by using a JASCO V-570 spectrophotometer. Luminescence spectra were recorded by using an Edinburgh Instrument spectrofluorometer. Transient absorption spectroscopy measurements were conducted using a custom laser spectrometer comprising a Continuum Surelite II Nd: YAG laser (fwhm = 8 ns) with a frequency tripled option (355 nm). Photomultiplier signals (kinetic traces) were processed by using a Teledyne LeCroy 604Zi (400 MHz, 20 GS/s) digital oscilloscope. SEM micrographs were obtained using an FE-SEM Jeol JSM 7600f scanning electron microscope with an accelerating voltage of 15 kV. ATR-FTIR spectra were collected with a Nicolet iS50 spectrometer (Thermo Fisher Scientific).

Materials Preparation. To improve the adhesion between FTO and WO_3, for both electrode types, a thin TiO_2 layer (thickness < 10 nm) and a WO_3 seed layer (thickness ≈ 200 nm) were deposited on top of the bare FTO. The former was prepared at room temperature via the slow hydrolysis of a 0.4 M aqueous solution of $TiCl_4$ in a closed chamber for 6 h, followed by calcination at 500 °C for 30 min. The WO_3 seed layer was obtained from a precursor solution cast on top of the TiO_2 adhesion layer before spin-coating deposition (for type I) or solvothermal growth (for type II). The WO_3 precursor solution was obtained by dissolving 0.46 g of metallic W in 5 mL of 35% H_2O_2 with continuous stirring overnight. Then, 2 drops of Triton X-100 were added, after which the solution was deposited on the underlayer via spin coating. After deposition, the electrodes were annealed at 550 °C for 40 min.

Synthesis of Type I Electrodes. 2.5 g of Na_2WO_4 were dissolved in 100 mL of distilled water. Subsequently, 20 mL of HCl were added to the solution to obtain tungstic acid. The excess of NaCl and HCl was eliminated by centrifuging the suspension followed by washing the resulting sediment with water. The process was repeated three times. The solid so obtained was dissolved at 60 °C in 5 mL of water with 2 g of oxalic acid. Subsequently, in the colloidal solution, the solid

https://doi.org/10.1021/acsaem.5c03321
ACS Appl. Energy Mater. 2025, 8, 18355−18362

copolymer PEG-BAE (polyethylene-glycol bisphenol A-epichlorohydrin) was added in a 1:5 ratio. After this step, 1 drop of Triton X-100 per 2 g of solution was added. Subsequently, the colloidal suspension was deposited on the WO_3 seed layer using a spin-coater. The desired thickness of the electrodes was obtained by repeating six depositions; each layer was annealed at 550 °C for 30 min. After the sixth deposition, the electrodes were annealed at 550 °C for 45 min. Finally, the electrodes were placed in a 1 M H_2SO_4 solution for 2 h, before being further heated in muffle at 550 °C for 45 min.

Synthesis of Type II Electrodes. 1.25 g amount of tungstic acid was dissolved at 95 °C in 10 mL of Milli-Q H_2O and 10 mL of 35% H_2O_2 under continuous stirring. A second solution was prepared composed of 1.2 g of oxalic acid dissolved in 18 mL of tungstic acid, 15 mL of Milli-Q H_2O, 60 mL of acetonitrile, and 3 mL of 6 M HCl. Subsequently, the two solutions were mixed, and the resulting solution was used to cover the TiO_2 under layer and WO_3 seed layer previously deposited on FTO. The electrodes were heated in an autoclave at 180 °C for 2 h. After these steps, the electrodes were washed with water and annealed at 500 °C for 2 h.

RESULTS AND DISCUSSION

Photoelectrochemical Characterization. The preparation of the colloidal (type I) and solvothermal (type II) WO_3 electrodes was performed following established literature protocols.[33−36] Type I electrodes were obtained through the deposition of a colloidal suspension (6 layer via spin-coating) to achieve a thickness of ca. 1.5 μm. The film shows a homogeneous distribution of spherical nanoparticles and is optically transparent (Scheme 1b).[34] On the other hand, type II electrodes were prepared via solvothermal growth of WO_3 on top of a thin TiO_2 seed layer (thickness < 10 nm).[35,36] The electrode surface is characterized by long leaves and lamellae (Scheme 1b). These structural features, combined with the larger thickness of the resulting electrodes (ca. 8 μm), endow type II electrodes with a substantially larger electrochemical surface active area when compared to type I electrodes.

We started our investigation by examining the possibility of oxidizing the CH and THF substrates under mild conditions using a simple electrolyte solution. Among the solvents tested, acetonitrile (0.1 M $LiClO_4$ as a supporting electrolyte) was considered as the medium of choice for the oxidation of CH (0.5 M concentration). On the other hand, effective oxidation of THF was not achieved in acetonitrile, and a pure THF solution (0.1 M $TBAPF_6$ as a supporting electrolyte) was thus employed.

The photoelectrochemical response of the WO_3 electrode was first assessed by recording $J-V$ curves under dark, light, and chopped irradiation conditions. The results obtained for both electrode types and substrates are collected in Figure 1. Detailed inspection of the traces shows that both electrodes deliver substantial photocurrent densities above 0.5 V vs Fc^+/Fc under illumination, which can be associated with the ability of the photogenerated holes to react with the organic substrates. More interestingly, with both CH and THF substrates, higher limiting photocurrent densities are observed for the solvothermal (type II) WO_3 electrodes (up to 1.6 and 1.8 mA·cm^{-2}, respectively) than the colloidal (type I) ones (up to 1.4 and 1.2 mA·cm^{-2}, respectively), most likely ensuing from the different morphology and the larger amount of active surface sites in the former than in the latter.[36]

The $J-V$ results were further complemented by measurements of the photon-to-current conversion efficiency spectra (IPCE and APCE). Figure 2 displays the IPCE results for both electrode types and substrates. Maximum values of ca. 60% in the range 350−400 nm are recorded in the presence of CH for

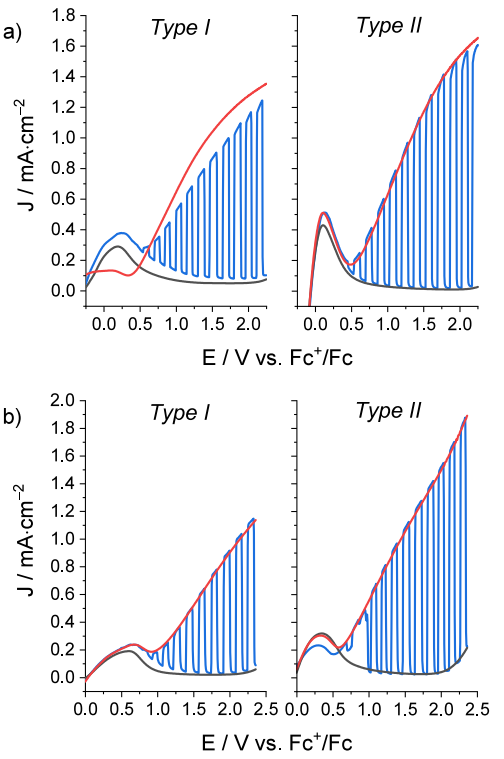

Figure 1. $J-V$ curves of type I and II electrodes in air-equilibrated (a) acetonitrile solution (0.1 M $LiClO_4$) containing 0.5 M CH and (b) THF solution (0.1 M $TBAPF_6$); irradiation was performed using a solar simulator calibrated at 1 sun (0.1 W·cm^{-2}).

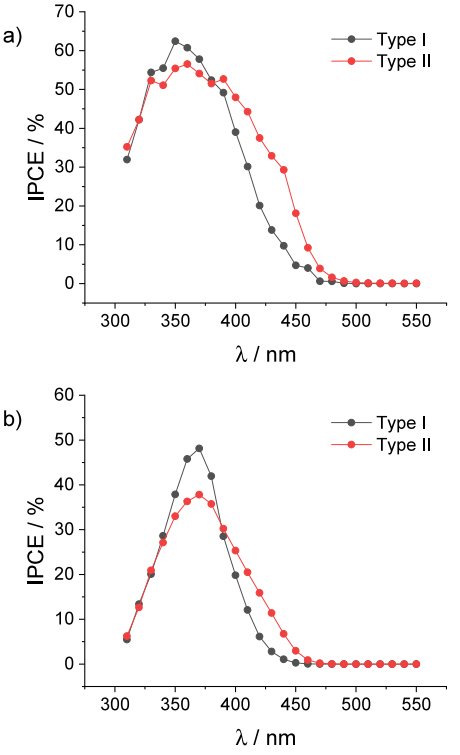

Figure 2. Photoaction spectra of type I and II electrodes in air-equilibrated (a) acetonitrile solution (0.1 M $LiClO_4$) containing 0.5 M CH and (b) THF solution (0.1 M $TBAPF_6$).

https://doi.org/10.1021/acsaem.5c03321
ACS Appl. Energy Mater. 2025, 8, 18355−18362

both type I and II electrodes, while lower values are registered in THF (40−50%) ostensibly due to the lower conductivity of the latter electrolyte and/or slower charge transfer rate.

Interestingly, the integrated IPCE spectra are always larger in the case of type II than type I electrodes, corroborating the results attained by $J-V$ measurements. Furthermore, with both organic substrates, the solvothermal electrodes display enhanced spectral response in the visible region between 400 and 450 nm. These results well correlate with those obtained for the same electrodes in aqueous electrolytes[36] and still confirm the superior photoelectrochemical response of type II over type I electrodes. Estimation of the APCE (Figures S3 and S4) further supports both the higher charge transfer and charge transport ability of type II electrodes upon photoirradiation in the visible spectral region.

Electrochemical impedance spectroscopy (EIS) was then employed to investigate in a more detailed manner the charge-transfer dynamics at the electrode−solution interface. The Nyquist plots (Figures S5−S8) are characterized by two main components (depressed semicircles), which can be associated with the charge transfer processes at the electrode/solution and FTO/WO_3 interfaces, respectively. The semiconductor/electrolyte interface is by far the dominant feature in the complex plane. Fitting of the experimental data according to a Randles circuit allows one to extract both the capacitance of the electrode/solution interface and the charge transfer resistance (see Supporting Information for all the experimental details concerning the EIS analysis). The resulting plots for both electrode types and organic substrates are collected in Figure 3.

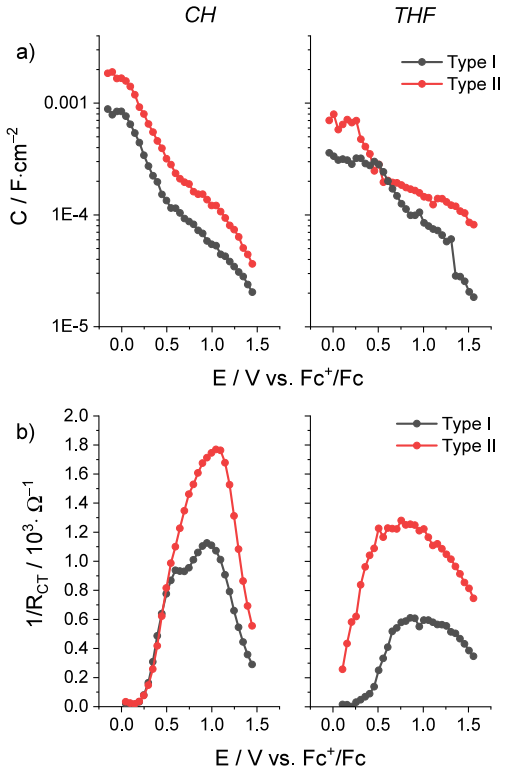

Figure 3. (a) Capacitive and (b) resistive curves of type I and II electrodes for the oxidation of 0.5 M CH in air-equilibrated acetonitrile solution (0.1 M $LiClO_4$) (left) and THF solution (0.1 M $TBAPF_6$) (right) obtained by EIS.

It can be noticed that, for both substrates, the capacitive curves (Figure 3a) show an appreciable exponential decay of the capacitance as a function of the applied potential, as expected for a chemical capacitance.[34,37] More interestingly, higher values are always measured for type II electrodes than for type I, consistent with the larger electrochemical surface active area. Similarly, for both CH and THF substrates, the resistive curves (Figure 3b) indicate that the charge transfer resistance is smaller in the case of the solvothermal electrodes than in the case of the colloidal ones. This can be understood considering the higher amount of surface sites in type II electrodes that promote more effective charge transfer processes at the electrolyte−solution interface. Overall, the EIS results well comply with the improved photoelectrochemical response recorded in $J-V$ mode (see above), suggesting a more pronounced tendency of type II over type I electrodes to promote the oxidation of organics, akin to what previously established in aqueous electrolytes.[34,37]

Photogeneration of Alcohols and Ketones. Once evaluated the potential ability of WO_3 electrodes toward the oxidation of CH and THF, we further examined the production of CH-ol and CH-one (from CH oxidation) or 2HTHF and GBL (from THF oxidation) by performing bulk electrolysis under continuous visible light irradiation (1 sun = 0.1 W·cm^{-2}) over a 6 h time frame. An external bias of +1.15 and +1.45 V vs Fc^+/Fc was applied for the oxidation of CH and THF, respectively. 7% H_2O was added at the catholyte in order to promote parallel hydrogen evolution and to avoid passivation of the Pt counter electrode. The results in terms of Faradaic efficiency (FE) are collected in Figure 4 for both electrode types and substrates (see Figures S15 and S16 for the kinetics of product formation). As regarding CH oxidation, though slightly larger amounts of photoproducts are attained with type II electrodes (mainly at shorter times), comparable FEs are in general estimated for both colloidal and solvothermal electrodes (e.g., 27% vs 28% for CH-one for type I and II electrodes, respectively, and 4% for CH-ol in both cases after 6 h of irradiation). This observation can be rationalized by assuming that the overall oxidation process is mainly determined by the interaction of the CH substrate with the electrode surface, which very likely resides in weak attractive forces between the electrode and the CH substrate because of the poor chemical affinity (i.e., polar W−OH sites vs apolar CH). For both electrode types, an appreciable decrease in the overall FE of product formation can be also recorded with increasing the photoreaction time from 3 to 6 h, which can be explained considering the possible participation of both CH-one and CH-ol in further oxidation reactions at the electrode surface.[23,31] Importantly, a comparison of the structural and morphological characteristics of pristine vs post-electrolysis electrodes demonstrates a remarkable stability and the absence of photocorrosion phenomena (see SI, Figures S21−S24). Furthermore, WO_3 electrodes subjected to electrolysis can be recycled after reconditioning (500 °C for 30 min), leading to similar product formation (Figures S29 and S30). The performances attained by our electrodes are consistent with those previously obtained by Sayama and co-workers,[31] showing how the replacement of the *t*BuOH/HNO_3 electrolyte with a simpler and safer acetonitrile solution proved successful. This might indeed represent a pivotal improvement that may open potential large-scale applications.

As to the oxidation of the THF substrate, colloidal electrodes efficiently deliver both 2HTHF and GBL with a

https://doi.org/10.1021/acsaem.5c03321
ACS Appl. Energy Mater. 2025, 8, 18355−18362

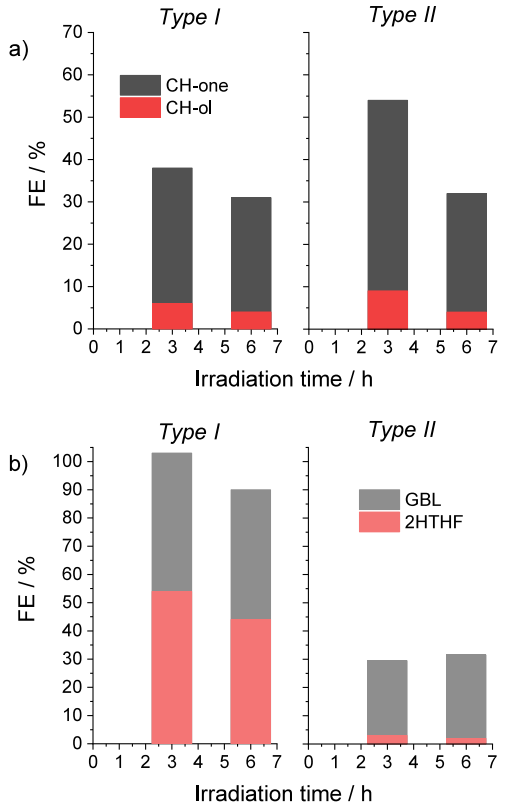

Figure 4. Faradaic efficiencies (FEs) of product formation for type I and II electrodes in air-equilibrated (a) acetonitrile solution (0.1 M $LiClO_4$) containing 0.5 M CH at +1.15 V vs Fc^+/Fc and (b) THF solution (0.1 M $TBAPF_6$) at +1.45 V vs Fc^+/Fc; irradiation was performed using a solar simulator calibrated at 1 sun (0.1 W·cm^{-2}).

total FE approaching 100% after 3 h of irradiation and only decreasing to 90% after 6 h. Product distribution is associated with an almost 2:1 alcohol:ketone ratio (Figure S18). Remarkably, photogeneration of both 2HTHF and GBL becomes substantially less efficient using solvothermal type II electrodes. For these latter, an overall FE of ca. 30% is attained for both products at both 3 and 6 h, with a dominating contribution from GBL (Figures 4b and S19). This trend substantially differs from that recorded for the oxidation of CH and can be explained by considering a preferential interaction between the THF substrate and the electrode surface. Under this assumption, we can hypothesize that the larger active surface area of type II over type I electrodes may favor a more rapid oxidation of the THF substrate as well as of the resulting oxidized products, leading to the generation of a higher amount of GBL over 2HTHF and a reduced total FE for the two products. Facile generation of additional degradation products from THF oxidation along the pathway toward complete mineralization is indeed not unexpected.[23] These results thus demonstrate that larger photocurrent densities do not necessarily translate to larger product yields. Even in this case, comparative analysis of pristine and post-electrolysis electrodes reveals exceptional stability and no signs of photocorrosion (Figures S25–S28). Similar performances were also recorded for recycled electrodes (Figures S31 and S32), still proving their stability under operational conditions.

A detailed analysis of the chronoamperometric profiles (Figures S15a, S16a, S18a, and S19a) points out a further difference between type I and II electrodes toward the oxidation of both organic substrates. Interestingly, stable photocurrent densities are appreciable in the case of colloidal electrodes over the whole time scale of the experiment (Figures S15a and S18a), whereas for the solvothermal WO_3, the photocurrents progressively decrease (Figures S16a and S19a). This evidence can be explained considering the possible involvement of passivation phenomena, likely implying adsorption of oxidation intermediates and byproducts under polarization at positive potentials. According to these findings, type I electrodes can also be considered the best choice in terms of photoelectrochemical stability in the chosen electrolyte.

In order to extract mechanistic information about the oxidation process, the photoreactions were also performed under N_2-purged conditions. Remarkably, photogeneration of both CH-ol or CH-one from CH oxidation was negligible, with recorded FEs < 1% (Figure S17). Similarly, with regard to oxidation of THF, no 2HTHF was detected under N_2, while only traces of GBL were observed (FE ∼ 3%, Figure S20). Thus, this evidence strongly points to a fundamental role of dioxygen in the overall oxidation process. Accordingly, and also based on literature precedents,[31] a mechanistic proposal can be formulated for the oxidation of CH and THF at the WO_3 surface.

$$WO_3 + h\nu \rightarrow {}^*WO_3(e^-, h^+) \quad (1)$$

$$R-H + h^+ \rightarrow R^{\cdot} + H^+ \quad (2)$$

$$R^{\cdot} + O_2 \rightarrow ROO^{\cdot} \quad (3)$$

$$2ROO^{\cdot} \rightarrow R-OH + R{=}O + O_2 \quad (4)$$

$$R-OH + 2h^+ \rightarrow R{=}O + 2H^+ \quad (5)$$

Photon absorption by the semiconductor is expected to yield an electron–hole pair (eq 1). While the electron is conveyed at the cathode to promote H_2 formation, the hole can reach the electrode–solution interface and oxidize a substrate molecule leading to a carbon-centered radical (eq 2). This process is expected to occur as a formal hydrogen atom transfer (HAT), likely mediated by a proton transfer to the electrode surface.[38] The carbon radical is then expected to react with O_2, leading to the formation of a peroxyl radical (eq 3). Further reaction of two peroxyl radicals finally delivers an equimolar amount of alcohol and ketone (CH-ol and CH-one for CH oxidation and 2HTHF and GBL for THF oxidation, eq 4). Additional oxidation of the alcohol to the ketone at the electrode surface (eq 5) can be also envisaged in order to support the typically largest amount of ketone product obtained in all experiments.

We should also consider that, in principle, the peroxyl radical might abstract a hydrogen atom from the CH or THF substrate, leading to the formation of a hydroperoxyl radical (eq 6). This latter may furnish an alternative mechanism to the formation of the R–OH product upon rupture of the O–O bond (eq 7) and subsequent reaction of the ensuing oxyl radical with the pristine substrate (eq 8).[39]

$$ROO^{\cdot} + R-H \rightarrow R-OOH + R^{\cdot} \quad (6)$$

$$R-OOH \rightarrow RO^{\cdot} + {}^{\cdot}OH \quad (7)$$

$$RO^{\cdot} + R-H \rightarrow ROH + R^{\cdot} \quad (8)$$

in order to verify this possibility, we tested the formation of hydroxyl radicals using a well-established fluorometric method based on the use of coumarin.[40] The failure to observe any

https://doi.org/10.1021/acsaem.5c03321
ACS Appl. Energy Mater. 2025, 8, 18355–18362

growing blue emission characteristic of 7-hydroxicoumarin upon irradiation of WO_3 powders in both 0.5 M CH in acetonitrile and THF strongly suggests that the reaction sequence in eqs 6−8 represents, if at all, a minor reaction pathway toward the photogeneration of the alcohol and ketone products.

Transient Absorption Spectroscopy. Laser flash photolysis (LFP) measurements (excitation at 355 nm) were conducted in order to extract further mechanistic insight into the primary photochemical processes initiating the oxidation of both CH and THF (eqs 1 and 2). For this reason, we focused our attention on the transient absorption signature of the photogenerated holes at 430 nm and its time evolution in pure acetonitrile, in acetonitrile in the presence of 0.5 M CH, and in pure THF solution. Due to the opaque nature of the solvothermal electrodes (see Scheme 1b), the spectroscopic analysis was limited solely to the colloidal type I electrodes. We believe that similar considerations can be, however, extrapolated for type II electrodes too. Figure 5 exhibits the corresponding kinetic traces recorded at different applied potentials. Under all experimental conditions, the amplitude of the transient absorption signal at 430 nm increases as a function of the applied bias. This is consistent with an increased concentration of photogenerated holes resulting from the gradual suppression of the electron/hole recombination at increasingly positive potentials.[34,41] The long-lived component of the photohole decay, spanning a time window between 1×10^{-4} and 1×10^{-1} s, contains kinetic information on the interfacial hole transfer process to the organic substrates. The decays were fitted using a Kohlrausch−Williams−Watts (KWW) stretched exponential function, which takes into account the statistical distribution of charge recombination rate constants resulting from the inherent inhomogeneity of the WO_3 surface.[34,41] From this fitting, a lifetime for the photogenerated holes was extracted under all of the conditions tested. A mean lifetime value was finally estimated for all the three electrolytes tested by averaging all the lifetimes estimated at different applied bias (see Supporting Information for further details). It can be noticed that in pure acetonitrile (deprived of the substrates), the decay of the photogenerated holes is almost complete in a time scale of ca. 50 ms, and an average lifetime of 3.8 ms can be estimated (Figure 5a). This value is appreciably shorter than that measured in water and other organic solvents,[34,41] pointing to the direct oxidation of acetonitrile at the illuminated WO_3 surface.[42] This observation agrees with the sizable photocurrent density measured in pure acetonitrile/0.1 M $LiClO_4$ (Figure S2).

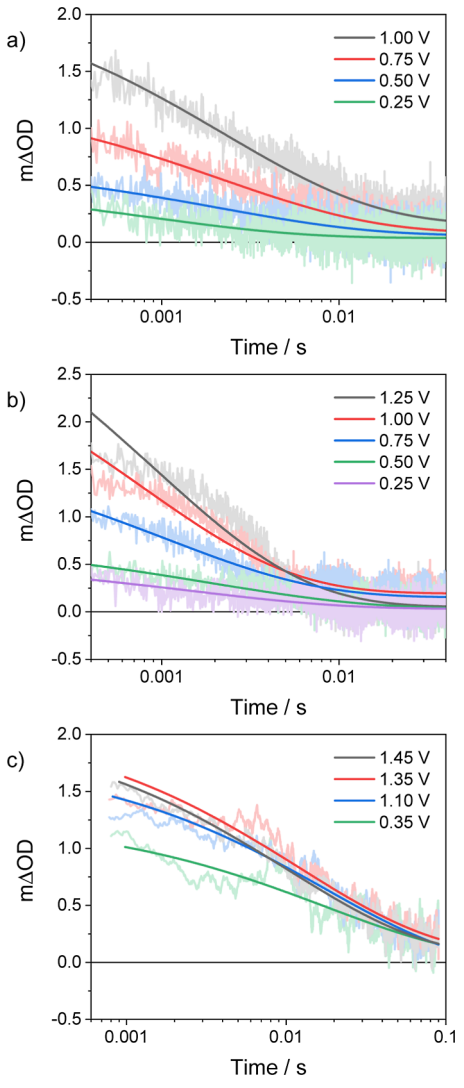

Figure 5. Kinetic traces at 430 nm at variable applied potentials measured by LFP (excitation at 355 nm) of type I electrodes in (a) pure acetonitrile solution (0.1 M $LiClO_4$), (b) acetonitrile solution (0.1 M $LiClO_4$) containing 0.5 M CH, and (c) THF solution (0.1 M $TBAPF_6$).

An important abatement of the average photohole lifetime (2.4 ms) is, however, detected upon addition of 0.5 M CH (Figure 5b), supporting a preferential reactivity toward the CH substrate and corroborating the observed photooxidation processes that lead to the formation of both CH-ol and CH-one, as previously discussed. Interestingly, the decay of the photogenerated holes in pure THF is substantially longer than that observed in acetonitrile, leading to an average lifetime of 28 ms (Figure 5c). This experimental evidence well complies with the failure to observe any 2HTHF and GBL photoproducts when the photooxidation of THF was attempted in acetonitrile as the solvent, where the latter outcompetes the former in hole scavenging.

CONCLUSIONS

We successfully employed WO_3 photoanodes and light to promote the oxidation of CH and THF to the respective alcohol and ketone. For this purpose, we have compared two WO_3 electrodes, featuring different structural morphology. One was obtained by deposition of a colloidal suspension (type I) and one via solvothermal growth (type II). The photoelectrochemical characterization of the photoanodes in organic solutions containing the target substrates shows improved performances for type II over type I electrodes, potentially arising from the larger electrochemical surface active area in the former. While this is not an issue for CH oxidation where a similar product distribution is obtained, it translates into a drawback when THF is employed as the substrate. In fact, for this latter, more efficient product formation is attained using type I electrodes, possibly resulting from overoxidation phenomena occurring with type II electrodes. Furthermore, contrarily to solvothermal electrodes, no noticeable photocurrent drop is apparent in the case of colloidal ones over a time frame of 6 h operation, still pointing

https://doi.org/10.1021/acsaem.5c03321
ACS Appl. Energy Mater. 2025, 8, 18355−18362

out their superior performance as far as the oxidation of both CH and THF under the present experimental conditions is concerned.

All in all, the results of the present work definitely confirm the possibility of using heterogeneous semiconductors, usually confined to applications in aqueous environments,[43−46] to target the oxidation of organics to value-added compounds. The results also demonstrate that the structural and morphological characteristics must be properly tuned when this approach is attempted. The possibility of generating a carbon-centered radical in a simple and sustainable manner using light may thus open a new avenue in the potential exploitation of heterogeneous semiconductors for the synthesis of organic molecules. Research in this direction is currently underway in our lab.

■ ASSOCIATED CONTENT

Supporting Information

The Supporting Information is available free of charge at https://pubs.acs.org/doi/10.1021/acsaem.5c03321.

Additional photoelectrochemical characterization, details of the bulk electrolysis experiments, electrode characterization before and after electrolysis, and additional laser flash photolysis data (PDF)

■ AUTHOR INFORMATION

Corresponding Author

Mirco Natali − *Department of Chemical, Pharmaceutical and Agricultural Sciences, University of Ferrara, Ferrara 44121, Italy;* orcid.org/0000-0002-6638-978X; Email: mirco.natali@unife.it

Authors

Andrea Mantovani − *Department of Chemical, Pharmaceutical and Agricultural Sciences, University of Ferrara, Ferrara 44121, Italy*

Edoardo Marchini − *Department of Chemical, Pharmaceutical and Agricultural Sciences, University of Ferrara, Ferrara 44121, Italy;* orcid.org/0000-0002-8092-1349

Anna Ianniello − *Department of Chemical, Pharmaceutical and Agricultural Sciences, University of Ferrara, Ferrara 44121, Italy*

Agnese Amati − *Department of Chemical, Pharmaceutical and Agricultural Sciences, University of Ferrara, Ferrara 44121, Italy;* Present Address: Warrant Hub— Tinexta Group, Corso Mazzini 11, 42015 Correggio (RE), Italy

Stefano Caramori − *Department of Chemical, Pharmaceutical and Agricultural Sciences, University of Ferrara, Ferrara 44121, Italy*

Complete contact information is available at: https://pubs.acs.org/10.1021/acsaem.5c03321

Author Contributions

The manuscript was written through contributions of all authors.

Notes

The authors declare no competing financial interest.

■ ACKNOWLEDGMENTS

Financial support from the Italian MUR (PRIN2020 project Electrolight4Value 2020927WY3) and the University of Ferrara (FAR2024) is gratefully acknowledged. Federico Droghetti and Marco Carmosino (University of Ferrara) are gratefully acknowledged for experimental assistance.

■ ABBREVIATIONS

CH, cyclohexane; CH-one, cyclohexanone; CH-ol, cyclohexanol; THF, tetrahydrofuran; GBL, gamma-butyrolactone; 2HTHF, 2-hydroxotetrahydrofuran; FE, Faradaic efficiency

■ REFERENCES

(1) Yaemsunthorn, K.; Kobielusz, M.; Macyk, W. Influence of TiO_2 Phases and Functional Groups on Photocatalytic Reduction of Nitroaromatics. *Catal. Today* **2024**, *432*, 114598.

(2) Alexander, B. D.; Augustynski, J. In *On Solar Hydrogen and Nanotechnology*, Vayssieres, L., Ed.: John Wiley & Sons 2009, 333−346.

(3) Sivula, K.; Le Formal, F.; Graetzel, M. Solar Water Splitting: Progress Using Hematite (α-Fe_2O_3) Photoelectrodes. *ChemSusChem* **2011**, *4*, 432−449.

(4) Chen, X.; Mao, S. S. Titanium Dioxide Nanomaterials: Synthesis, Properties, Modifications, and Application. *Chem. Rev.* **2007**, *107*, 2891−2959.

(5) Alini, S.; Babini, P. The Industrial Oxidation of KA Oil to Adipic Acid. *Handbook of Advanced Methods and Processes in Oxidation Catalysis*; World Scientific, 2014, pp 320−333.

(6) Natali, M.; Sartorel, A.; Ruggi, A. Beyond Water Oxidation: Hybrid, Molecular-Based Photoanodes for the Production of Value-Added Organics. *Front. Chem.* **2022**, *10*, 907510.

(7) Li, S.; Li, Z.-J.; Yu, H.; Sytu, M. R.; Wang, Y.; Beeri, D.; Zheng, W.; ShermanYooLeem, B. D. C. G. G. D.; Yoo, C. G.; Leem, G. Solar-Driven Lignin Oxidation via Hydrogen Atom Transfer with a Dye-Sensitized TiO_2 Photoanode. *ACS Energy Lett.* **2020**, *5*, 777−784.

(8) Pati, P. B.; Abdellah, M.; Diring, S.; Hammarström, L.; Odobel, F. Molecular Triad Containing a TEMPO Catalyst Grafted on Mesoporous Indium Tin Oxide as a Photoelectrocatalytic Anode for Visible Light-Driven Alcohol Oxidation. *ChemSusChem* **2021**, *14*, 2902−2913.

(9) Yang, Y.; Volpato, G. A.; Rossin, E.; Peruffo, N.; Tumbarello, F.; Nicoletti, C.; Bonetto, R.; Paoloni, L.; Umari, P.; Colusso, E.; Dell'Amico, L.; Berardi, S.; Collini, E.; Caramori, S.; Agnoli, S.; Sartorel, A. Photoelectrochemical C−H Activation Through a Quinacridone Dye Enabling Proton-Coupled Electron Transfer. *ChemSusChem* **2023**, *16*, No. e202201980.

(10) Turlington, M. D.; Ahmed, S.; Schanze, K. S. Radical Cation Diels−Alder Reaction by Photocatalysis at a Dye Sensitized Photoanode. *ACS Catal.* **2024**, *14*, 12512−12517.

(11) Wei, H. L.; Liu, S. E.; Li, G. X.; Su, Y. H.; Yan, W. C.; Luo, Z. H. Numerical Modeling of a Microreactor for the Synthesis of Adipic Acid Via KA Oil Oxidation. *Chem. Eng. Sci.* **2021**, *230*, 116208.

(12) Wang, J.; Yang, J.; Zeng, S.; Liu, H.; Li, F.; Xie, H.; Tang, S.; Fu, Z.; Li, Y. Efficient Photocatalytic Oxidation of Cyclohexane to KA Oil by Carbon Nitride Hybridized Decatungstate under Visible Light. *J. Catal.* **2025**, *443*, 115996.

(13) Gill, A. M.; Hinde, C. S.; Leary, R. K.; Potter, M. E.; Jouve, A.; Wells, P. P.; Midgley, P. A.; Thomas, J. M.; Raja, R. Design of Highly Selective Platinum Nanoparticle Catalysts for the Aerobic Oxidation of KA-Oil using Continuous-Flow Chemistry. *ChemSusChem* **2016**, *9*, 423−427.

(14) Wei, Y.; You, K.; Li, W.; Xu, W.; Zhao, F.; Yan, D.; Zhang, X.; Chen, Z.; Luo, H. Highly-dispersed Ni_3Fe Alloy Nanoparticles Anchored on MgAl-LDO for Efficient Catalytic Amination of KA-Oil to Cyclohexylamine. *J. Catal.* **2024**, *430*, 115315.

(15) Lorenzo, D.; Galvan, C. D.; Triana, C.; Santos, A.; Romero, A.; Bogle, I. D. L. Modelling of a Reactive Distillation in the Production Process of High Purity Cyclohexanone to Produce Caprolactam. *Comput.-Aided Chem. Eng.* **2016**, *38*, 176−181.

(16) Moore, T.; Adhikari, R.; Gunatillake, P. Chemosynthesis of Bioresorbable Poly(γ-butyrolactone) by Ring-Opening Polymerisation: a Review. *Biomaterials* **2005**, *26*, 3771−3782.
(17) Hemminki, K. Reactions of β-Propiolactone, β-Butyrolactone and γ-Butyrolactone with Nucleic Acids. *Chem.-Biol. Interact.* **1981**, *34*, 323−331.
(18) Bhanushali, J. T.; Prasad, D.; Patil, K. N.; Babu, G. V. R.; Kainthla, I.; Rao, K. S. R.; Jadhav, A. H.; Nagaraja, B. M. The selectively regulated vapour phase dehydrogenation of 1,4-butanediol to γ-butyrolactone employing a copper-based ceria catalyst. *New J. Chem.* **2019**, *43*, 11968−11983.
(19) Yoon, Y.-S.; Shin, H. K.; Kwak, B. S. Ring Conversion of γ-Butyrolactone Into *N*-Methyl-2-Pyrrolidone Over Modified Zeolites. *Catal. Commun.* **2002**, *3*, 349−355.
(20) Shimasaki, Y.; Yano, H.; Sugiura, H.; Kambe, H. Development of a New Production Process for N-Vinyl-2-pyrrolidone. *Bull. Chem. Soc. Jpn.* **2008**, *81*, 449−459.
(21) Abduh, N. A. Y.; Al-Kahtani, A.; Algarni, T. S.; Al-Odayni, A. S. Selective Oxidation of Tetrahydrofuran to Gamma-Butyrolactone over Spinel $ZnFe_2O_4$ Nanoparticle Catalyst. *Catalysts* **2023**, *13*, 692.
(22) Fornal, E.; Giannotti, C. Photocatalyzed Oxidation of Cyclohexane with Heterogenized Decatungstate. *J. Photochem. Photobiol., A* **2007**, *188*, 279−286.
(23) Feng, Y.; Jia, C.; Zhao, H.; Wang, K.; Wang, X. Phase-Dependent Photocatalytic Selective Oxidation of Cyclohexane over Copper Vanadates. *New J. Chem.* **2022**, *46*, 4082.
(24) Mehrvar, M.; Anderson, W. A.; Moo-Young, M. Photocatalytic Degradation of Aqueous Tetrahydrofuran, 1,4-Dioxane, and Their Mixture with TiO_2. *Int. J. Photoenergy* **2000**, *2*, 67−80.
(25) Hata, E.; Takal, T.; Mukaiyama, T. Oxygenation of Tetrahydrofurans with Combined Use of Molecular Oxygen and ALPHA-Diketone Catalyzed by Cobalt(III) Complex. *Chem. Lett.* **1993**, *22* (9), 1513−1516.
(26) Luo, Y. R. *Handbook of Bond Dissociation Energies in Organic Compounds*; CRC Press, 2002; Vol. *1*, p 392.
(27) Almquist, C. B.; Biswas, P. The Photo-Oxidation of Cyclohexane on Titanium Dioxide: An Investigation of Competitive Adsorption and its Effects on Product Formation and Selectivity. *Appl. Catal., A* **2001**, *214*, 259−271.
(28) Padmalatha, P.; Khatri, P. K.; Jain, S. L. Selenium-Doped TiO_2 as an Efficient Photocatalyst for the Oxidation of Tetrahydrofuran to γ-Butyrolactone Using Hydrogen Peroxide as Oxidant. *Synlett* **2013**, *24*, 1405−1409.
(29) Xu, G.; Zhang, Y.; Liu, P.; Deng, Q.; Ma, Y.; Zuo, C.; Chunling, M. N-P25-assisted MIL-125 Derived Porous Nitrogen Doped and Carbon Modified TiO_2 Mixed-Phase Junction Photocatalyst for KA oil Synthesis. *J. Photochem. Photobiol., A* **2023**, *452*, 115578.
(30) Shiraishi, Y.; Sugano, Y.; Ichikawa, S.; Hirai, T. Visible Light-Induced Partial Oxidation of Cyclohexane on WO_3 Loaded with Pt Nanoparticles. *Catal. Sci. Technol.* **2012**, *2*, 400−405.
(31) Tateno, H.; Iguchi, S.; Misechi, Y.; Sayama, K. Photo-Electrochemical C−H Bond Activation of Cyclohexane Using a WO_3 Photoanode and Visible Light. *Angew. Chem., Int. Ed.* **2018**, *57*, 11238−11241.
(32) Inoue, R.; Yamaguchi, M.; Murakami, Y.; Okano, K.; Mori, A. Revisiting of Benzophenone Ketyl Still: Use of a Sodium Dispersion for the Preparation of Anhydrous Solvents. *ACS Omega* **2018**, *3*, 12703−12706.
(33) Solarska, R.; Alexander, B. D.; Augustynski, J. Electrochromic and Structural Characteristics of Mesoporous WO_3 Films Prepared by a Sol-gel Method. *J. Solid State Electrochem.* **2004**, *8*, 748−756.
(34) Cristino, V.; Marinello, S.; Molinari, A.; Caramori, S.; Carli, S.; Boaretto, R.; ArgazziMeda, R. L.; Bignozzi, C. A.; Bignozzi, C. A. Some Aspects of the Charge Transfer Dynamics in Nanostructured WO_3 Films. *J. Mater. Chem. A* **2016**, *4*, 2995−3006.
(35) Su, J.; Feng, X.; Sloppy, J. D.; Guo, L.; Grimes, C. A. Vertically Aligned WO_3 Nanowire Arrays Grown Directly on Transparent Conducting Oxide Coated Glass: Synthesis and Photoelectrochemical Properties. *Nano Lett.* **2011**, *11*, 203−208.
(36) Cescon, M.; Stevanin, C.; Ardit, M.; Orlandi, M.; Martucci, A.; Chenet, T.; Pasti, L.; Caramori, S.; Cristino, V. Solvothermally Grown Oriented WO_3 Nanoflakes for the Photocatalytic Degradation of Pharmaceuticals in a Flow Reactor. *Nanomaterials* **2024**, *14*, 860.
(37) Bignozzi, C. A.; Caramori, S.; Cristino, V.; Argazzi, R.; Meda, L.; Tacca, A. Nanostructured Photoelectrodes Based on WO_3: Applications to Photooxidation of Aqueous Electrolytes. *Chem. Soc. Rev.* **2013**, *42*, 2228−2246.
(38) Schrauben, J. N.; Hayoun, R.; Valdez, C. N.; Braten, M.; Fridley, L.; Mayer, J. M. Titanium and Zinc Oxide Nanoparticles are Proton-Coupled Electron Transfer Agents. *Science* **2012**, *336*, 1298−1301.
(39) Vomeri, A.; Stucchi, M.; Villa, A.; Evangelisti, C.; Beck, A.; Prati, L. New Insights for the Catalytic Oxidation of Cyclohexane to K-A Oil. *J. Energy Chem.* **2022**, *70*, 45−51.
(40) Czili, H.; Horvath, A. Applicability of Coumarin for Detecting and Measuring Hydroxyl Radicals Generated by Photoexcitation of TiO_2 Nanoparticles. *Appl. Catal., B* **2008**, *81*, 295−302.
(41) Vecchi, P.; Ruani, P.; Mazzanti, M.; Loague, Q. R.; Mazzaro, R.; Boscherini, F.; Ventura, B.; Meyer, G. J.; Armaroli, N.; Caramori, S.; Pasquini, L. Impact of Co−Fe Overlayers on Charge Carrier Dynamics at WO_3/$BiVO_4$ Heterojunctions: A Picosecond-to-Second Spectroscopic Analysis. *ACS Energy Lett.* **2024**, *9*, 2193−2200.
(42) Mi, Q.; Coridan, R. H.; Brunschwig, B. S.; Gray, H. B.; Lewis, N. S. Photoelectrochemical Oxidation of Anions by WO_3 in Aqueous and Nonaqueous Electrolytes. *Energy Environ. Sci.* **2013**, *6*, 2646−2653.
(43) Liu, X.; Wang, F.; Wang, Q. Nanostructure-based WO_3 Photoanodes for Photoelectrochemical Water Splitting. *Phys. Chem. Chem. Phys.* **2012**, *14*, 7894−7911.
(44) Wang, Y.; Tian, W.; Chen, C.; Xu, W.; Li, L. Tungsten Trioxide Nanostructures for Photoelectrochemical Water Splitting: Material Engineering and Charge Carrier Dynamic Manipulation. *Adv. Funct. Mater.* **2019**, *29*, 1809036.
(45) Klepser, B.; Bartlett, B. M. Anchoring a Molecular Iron Catalyst to Solar-Responsive WO_3 Improves the Rate and Selectivity of Photoelectrochemical Water Oxidation. *J. Am. Chem. Soc.* **2014**, *136*, 1694−1697.
(46) Rosser, T. E.; Gross, M. A.; Lai, Y. H.; Reisner, E. Precious-Metal Free Photoelectrochemical Water Splitting with Immobilised Molecular Ni and Fe Redox Catalysts. *Chem. Sci.* **2016**, *7*, 4024−4035.

https://doi.org/10.1021/acsaem.5c03321
ACS Appl. Energy Mater. 2025, 8, 18355−18362